Unitary Quantum Lattice Algorithms for Turbulence

George Vahala
COLLEGE OF WILLIAM & MARY THE

05/23/2016
Final Report

REPORT DOCUMENTATION PAGE

1. REPORT DATE *(DD-MM-YYYY)*	2. REPORT TYPE	3. DATES COVERED *(From - To)*
12-05-2016	FINAL	15 Feb 2013 - 14 Feb 2016

4. TITLE AND SUBTITLE

"Unitary Quantum Lattice Algorithms for Turbulence"

5a. CONTRACT NUMBER

5b. GRANT NUMBER

FA9550-13-1-0038

5c. PROGRAM ELEMENT NUMBER

6. AUTHOR(S)

George Vahala, Linda Vahala

5d. PROJECT NUMBER

5e. TASK NUMBER

5f. WORK UNIT NUMBER

7. PERFORMING ORGANIZATION NAME(S) AND ADDRESS(ES)

College of William & Mary
261 Richmond Rd
Williamsburg, VA 23185-4042

8. PERFORMING ORGANIZATION REPORT NUMBER

AFOSR-FA9550-3

9. SPONSORING/MONITORING AGENCY NAME(S) AND ADDRESS(ES)

USAF, AFRL
AF Office of Scientific Research 875
North Randolph Street, Rm 312
Arlington, VA 22203

10. SPONSOR/MONITOR'S ACRONYM(S)

11. SPONSOR/MONITOR'S REPORT NUMBER(S)

12. DISTRIBUTION/AVAILABILITY STATEMENT

For public distriubtion

13. SUPPLEMENTARY NOTES

14. ABSTRACT

A qubit unitary lattice algorithm is developed for the mean field evolution of the ground state of a Bose-Einstein condensate – whether in a magnetic or optical trap. The algorithm consists of interleaved collide-stream operators which in diffusion ordering recovers the spinor Gross Pitaevskii equations and is ideally parallelized. The algorithm is benchmarked against exact one dimensional vector inelastic soliton collision solutions. Three dimensional quantum turbulence is examined for scalar Bose Einstein condensates and the compressible kinetic energy spectrum exhibits three different cascades –

15. SUBJECT TERMS

qubits, unitary operators, quantum lattice gas, Bose Einstein Condenstates, quantum vortices, turbulence

16. SECURITY CLASSIFICATION OF:			17. LIMITATION OF ABSTRACT	18. NUMBER OF PAGES	19a. NAME OF RESPONSIBLE PERSON
a. REPORT	b. ABSTRACT	c. THIS PAGE			George Vahala
U	U	U	UU	20	19b. TELEPHONE NUMBER *(Include area code)* 757/221-3528

INSTRUCTIONS FOR COMPLETING SF 298

1. REPORT DATE. Full publication date, including day, month, if available. Must cite at least the year and be Year 2000 compliant, e.g. 30-06-1998; xx-06-1998; xx-xx-1998.

2. REPORT TYPE. State the type of report, such as final, technical, interim, memorandum, master's thesis, progress, quarterly, research, special, group study, etc.

3. DATE COVERED. Indicate the time during which the work was performed and the report was written, e.g., Jun 1997 - Jun 1998; 1-10 Jun 1996; May - Nov 1998; Nov 1998.

4. TITLE. Enter title and subtitle with volume number and part number, if applicable. On classified documents, enter the title classification in parentheses.

5a. CONTRACT NUMBER. Enter all contract numbers as they appear in the report, e.g. F33315-86-C-5169.

5b. GRANT NUMBER. Enter all grant numbers as they appear in the report. e.g. AFOSR-82-1234.

5c. PROGRAM ELEMENT NUMBER. Enter all program element numbers as they appear in the report, e.g. 61101A.

5e. TASK NUMBER. Enter all task numbers as they appear in the report, e.g. 05; RF0330201; T4112.

5f. WORK UNIT NUMBER. Enter all work unit numbers as they appear in the report, e.g. 001; AFAPL30480105.

6. AUTHOR(S). Enter name(s) of person(s) responsible for writing the report, performing the research, or credited with the content of the report. The form of entry is the last name, first name, middle initial, and additional qualifiers separated by commas, e.g. Smith, Richard, J, Jr.

7. PERFORMING ORGANIZATION NAME(S) AND ADDRESS(ES). Self-explanatory.

8. PERFORMING ORGANIZATION REPORT NUMBER. Enter all unique alphanumeric report numbers assigned by the performing organization, e.g. BRL-1234; AFWL-TR-85-4017-Vol-21-PT-2.

9. SPONSORING/MONITORING AGENCY NAME(S) AND ADDRESS(ES). Enter the name and address of the organization(s) financially responsible for and monitoring the work.

10. SPONSOR/MONITOR'S ACRONYM(S). Enter, if available, e.g. BRL, ARDEC, NADC.

11. SPONSOR/MONITOR'S REPORT NUMBER(S). Enter report number as assigned by the sponsoring/ monitoring agency, if available, e.g. BRL-TR-829; -215.

12. DISTRIBUTION/AVAILABILITY STATEMENT. Use agency-mandated availability statements to indicate the public availability or distribution limitations of the report. If additional limitations/ restrictions or special markings are indicated, follow agency authorization procedures, e.g. RD/FRD, PROPIN, ITAR, etc. Include copyright information.

13. SUPPLEMENTARY NOTES. Enter information not included elsewhere such as: prepared in cooperation with; translation of; report supersedes; old edition number, etc.

14. ABSTRACT. A brief (approximately 200 words) factual summary of the most significant information.

15. SUBJECT TERMS. Key words or phrases identifying major concepts in the report.

16. SECURITY CLASSIFICATION. Enter security classification in accordance with security classification regulations, e.g. U, C, S, etc. If this form contains classified information, stamp classification level on the top and bottom of this page.

17. LIMITATION OF ABSTRACT. This block must be completed to assign a distribution limitation to the abstract. Enter UU (Unclassified Unlimited) or SAR (Same as Report). An entry in this block is necessary if the abstract is to be limited.

FINAL REPORT

Grant FA9550-13-1-0038

Unitary Quantum Lattice Algorithms for Turbulence

2014-2016

George Vahala
William & Mary

Linda Vahala
Old Dominion University

We have been investigating the application of unitary quantum lattice algorithms for the evolution of quantum turbulence in Bose Einstein condensates (BEC) [1]-[[20].   The Hamiltonian for the cold atom BEC trapped in a magnetic well under the mean field approximation is given by

$$H = \int d^3x \left[\psi^* \left(-\nabla^2 + V_{ext} \right) \psi + \frac{1}{2} g |\psi|^4 \right] \tag{1}$$

and this gives rise to the scalar Gross-Pitaevskii (GP) equation for the wave function (with $\hbar = 1 = m$)

$$i \frac{\partial \psi}{\partial t} = \frac{\delta H}{\delta \psi^*} = \left[-\nabla^2 + V_{ext} + g |\psi|^2 \right] \psi \tag{2}$$

The superfluid (mean) velocity of the BEC can be discerned from the continuity equation

$$\frac{\partial \rho}{\partial t} + \nabla \bullet \left(\rho \mathbf{v}_{BEC} \right) = 0 \tag{3}$$

where the density $\rho = \psi \psi^*$. From the GP equation, we thus obtain

$$\rho \mathbf{v}_{BEC} = i \left(\psi^* \nabla \psi - \psi \nabla \psi^* \right) \tag{4}$$

From the Madelung transformation (for winding number n_w)

$$\psi = \sqrt{\rho} \, \exp \left[i n_w \varphi \right] \tag{5}$$

one connects the phase of the wave function with the mean superfluid velocity

$$\mathbf{v}_{BEC} = 2 n_w \nabla \varphi \tag{6}$$

While this leads to $\nabla \times \mathbf{v}_{BEC} = 0$, there is no circulation for simply connected domains:

$$\oint_C d\vec{\ell} \bullet \mathbf{v}_{BEC} = 0 \quad : \text{ if domain is simplify connected} \tag{9}$$

However, it has been found experimentally that in sufficiently rotated BECs or He4, one does find quantized circulations.   Hence we must be dealing with a multi-connected domain so that

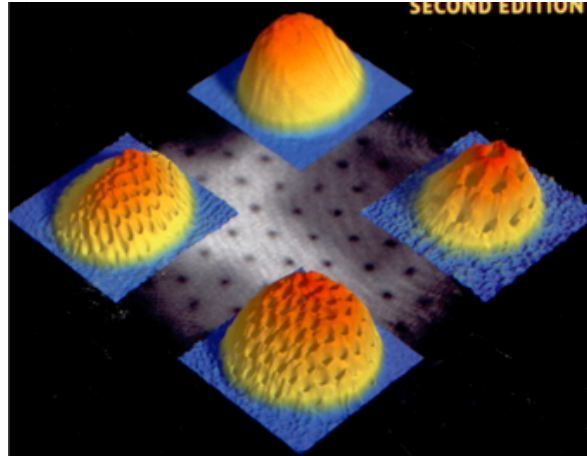*Fig. 1 Various scalar BEC densities under rotation (experiment) :(a) top plot – non-rotating BEC density; (b) plot-to-the-right : rotating BEC, with 16 steady state quantized vortices (the "holes" are the vortex cores); (c) bottom-plot : more rapidly rotating BEC with 70 vortices in lattice formation, (d) plot-to-the-left : most rapidly rotating BEC with 130 vortices in lattice formation.*

$$\oint_C d\vec{\ell} \cdot \mathbf{v}_{BEC} \neq 0 \quad , \tag{10}$$

with topological singularities

$$\rho(x_c) = 0 \tag{11}$$

and quantization of circulation about these singularities

$$\oint d\vec{\ell} \cdot \mathbf{v}_{BEC} = n_w \kappa \tag{12}$$

where κ is the quantization of circulation. Thus, for rotating scalar BECs one finds singular quantized vortices with zero density at the cores. This is what is seen experimentally, in Fig. 1.

In an early simulation we chose as an initial condition a winding number $n_w = 6$ singular line vortex core. This is a highly unstable initial condition since the energy of the 6-fold degenerate line vortex is greater than 6 times the energy of a winding-number-1 line vortex. One finds vortex reconnection and tanglement – which Feynman defined as quantum turbulence.
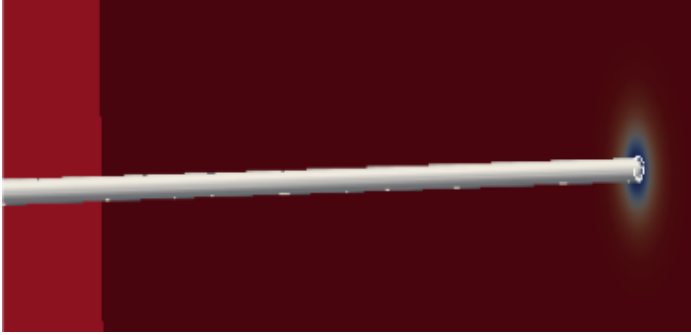
(a) t = 0   6-fold degenerate line vortex core
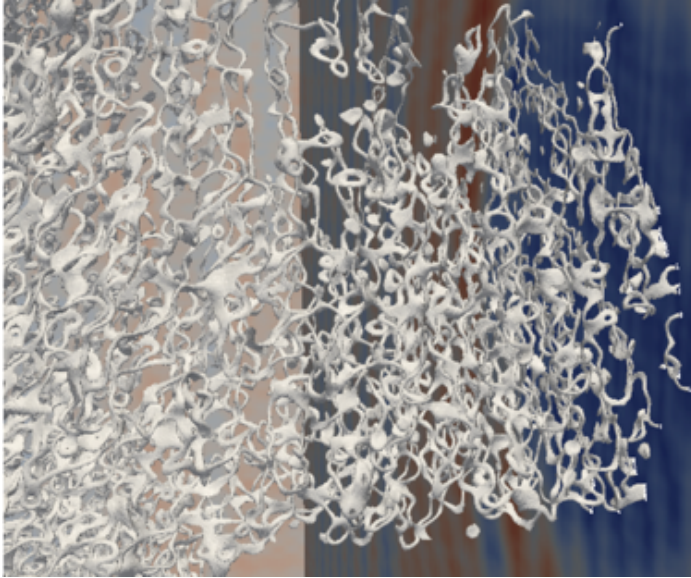
(b) reconnection and vortex tangles at later time
 Fig. 2   Tanglement and reconnection of a degenerate scalar quantum line vortex.

It is of interest to discuss the relationship between quantum turbulence spectra and that for classical fluid turbulence. Typically, classical fluid turbulence is discussed for incompressible turbulence, with the Kolmogorov $k^{-5/3}$ kinetic energy spectrum. Clearly, since compressibility

plays an important role in quantum turbulence (since a scalar singular quantum vortex has zero density for its core and then asymptotes to a constant density in a healing length) there should be some differences. In a simulation on 5760^3-grid, we found the total kinetic energy spectrum has a triple cascade
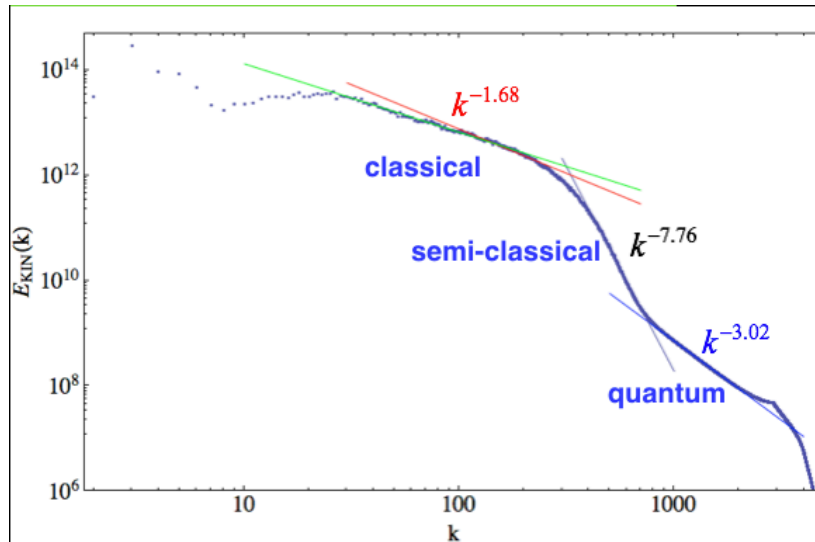
Fig. 3 The total kinetic energy spectrum for scalar quantum turbulence

In this (CAP-2) run, we did not have enough time to separate the incompressible from the compressible kinetic energies (see Fig. 5 for such a separation on a smaller grid of 3072^3) – but the existence of a triple cascade region is typical of multi-scale physics. For example, solar wind data
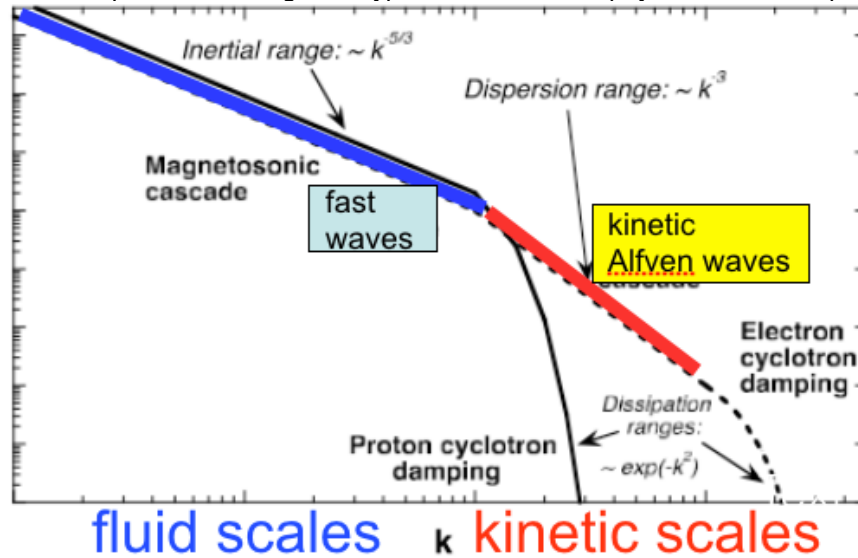
Fig, 4 Magnetic energy spectrum from solar wind data exhibiting 2 cascades: fluid (small k) scales exhibiting the $k^{-5/3}$ spectrum, and a kinetic scales spectrum of k^{-3} from the kinetic (large k) scales.

It is tempting to associate the small k $k^{-5/3}$-spectrum in Fig. 3 with classical turbulence scales, the intermediate sharp cascade with semi-classical physics, and the large k k^{-3} spectrum with quantum cascades. It should also be pointed out the significance difference between classical and quantum turbulence: in classical turbulence it is essential that the fluid be dissipative – i.e., non-zero

viscosity. On the other hand, the scalar BEC is a Hamiltonian system with energy conservation. Indeed, using the Madelung transformation one can rewrite the GP equation into the more familiar continuity and momentum equations and then identify the compressible, incompressible and quantum kinetic energies. We have performed detailed spectral analysis on a quantum turbulence run on 3072^3-grid for both non-degenerate ($n_w = 1$) and degenerate ($n_w = 2$) linear vortex cores.
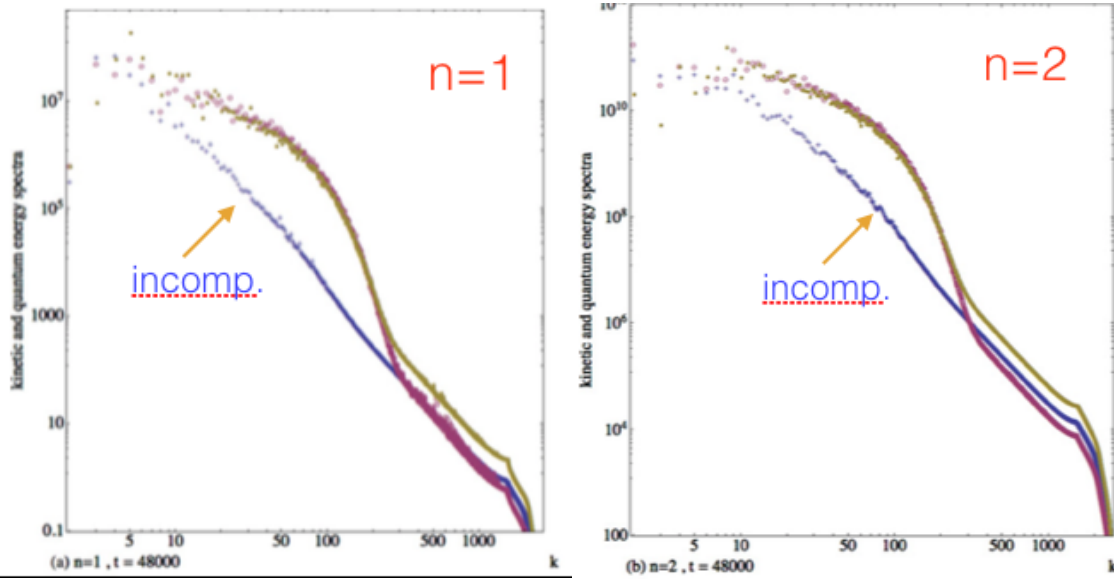
Fig. 5 The energy spectra for two different set of initial conditions on the linear vortex cores : (a) $n_w = 1$, and (b) $n_w = 2$. The more turbulence state (b) gives rise to 'cleaner' spectra. The blue curve – incompressible kinetic energy spectrum, red curve – compressible kinetic energy spectrum, gold curve – quantum kinetic energy spectrum

Some significant outcomes from these simulations:

(a) the incompressible energy spectrum $E_{inc}(k) << E_{comp}(k), E_{qu}(k)$ for $k < 200$,

(b) for nearly the complete spectral range, $30 < k < 1000$, $E_{inc}(k) \sim k^{-3}$. There is basically a single cascade in the incompressible kinetic energy – with no sign of a Kolmogorov region.

(c) both the compressible and quantum kinetic energies exhibit a 3-cascade spectrum:

$$\text{small } k : \quad E_{comp}(k) \sim k^{-5/3} , \quad E_{qu}(k) \sim k^{-5/3}$$

$$\text{intermediate } k: \quad E_{comp}(k) \sim k^{-8} , \quad E_{qu}(k) \sim k^{-8}$$

$$\text{large } k : \quad E_{comp}(k) \sim k^{-3} , \quad E_{qu}(k) \sim k^{-3}$$

Unitary Quantum Lattice Gas Algroithm (QLG)

Quantum entanglement is the backbone of quantum computing and quantum information theory, with qubits as the building blocks. Unlike the classical bit (which can take on either the value '0' or '1'), and the classical Pbit (which can take on a probability between '0' and '1'), the qubit state exists on the unit sphere with

$$|q\rangle = \gamma_0 |0\rangle + \gamma_1 |1\rangle , \quad with \quad |\gamma_0|^2 + |\gamma_1|^2 = 1 \tag{13}$$

where γ_0 and γ_1 are complex probability amplitudes.

Fig. 6 The classical bit, the probability bit and the qubit.

For quantum entanglement, one requires at least two qubits:

$$\left|q_1q_2\right\rangle = \gamma_{00}\left|00\right\rangle + \gamma_{01}\left|01\right\rangle + \gamma_{10}\left|10\right\rangle + \gamma_{11}\left|11\right\rangle , \tag{14}$$
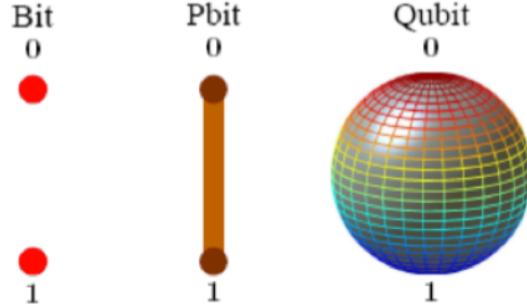
We then apply an intertwined set of non-commuting unitary collision and streaming operators so that we recover the finite difference form of the scalar GP equation (2) on a simple cubic lattice. In this mesoscopic approach we consider the spinor

$$\left|\phi(\mathbf{x},t)\right\rangle = \begin{pmatrix} \gamma_{01}(\mathbf{x},t) \\ \gamma_{10}(\mathbf{x},t) \end{pmatrix} \tag{15}$$

as a representation of the scalar wave function $\psi(\mathbf{x},t)$. In particular, we consider the unitary collision operator, based on the 3D relativistic Dirac particle dynamics theory of Yepez,

$$\hat{C}_D = \begin{pmatrix} \cos\theta(\mathbf{x}) & -i\sin\theta(\mathbf{x}) \\ -i\sin\theta(\mathbf{x}) & \cos\theta(\mathbf{x}) \end{pmatrix} , \quad \text{with } \theta(\mathbf{x}) = \frac{\pi}{4} - \frac{1}{24}\Omega(\mathbf{x}) \tag{16}$$

and the unitary streaming operator (an exponential of spin-1/2 matrics) which is basically just a shift operator on the individual spinor components of Eq. (15)

$$\hat{S}_{\Delta x,0}\left|\phi(\mathbf{x})\right\rangle = \begin{pmatrix} \gamma_{01}(\mathbf{x}+\Delta\mathbf{x}) \\ \gamma_{10}(\mathbf{x}) \end{pmatrix} , \quad \hat{S}_{\Delta x,1}\left|\phi(\mathbf{x})\right\rangle = \begin{pmatrix} \gamma_{01}(\mathbf{x}) \\ \gamma_{10}(\mathbf{x}+\Delta\mathbf{x}) \end{pmatrix} . \tag{17}$$

The unitary collision operator locally entangles the qubit amplitudes at each nodal site while the unitary streaming operator spreads this entanglement throughout the lattice. The non-commuting interleaved sequence of collide-streams give rise to our QLG mesoscopic finite difference algorithm:

$$\left|\phi(\mathbf{x},t+\Delta t)\right\rangle = \hat{U}[\mathbf{x},\Omega]\left|\phi(\mathbf{x},t)\right\rangle \tag{18}$$

where the evolution operator

$$\hat{U}[\mathbf{x},\Omega] = \hat{J}_{x0}^2 \hat{J}_{y1}^2 \hat{J}_{z0}^2 \hat{J}_{z1}^2 \hat{J}_{y0}^2 \hat{J}_{x1}^2 \quad \text{and} \quad \hat{J}_{x0} = \hat{S}_{-\Delta x,0}\hat{C}_D.\hat{S}_{+\Delta x,0}\hat{C}_D \tag{19}$$

While Eqs. (16)-(20) is the mesoscopis algorithm solved on the supercomputers, for as yet unspecified $\Omega(\mathbf{x})$, it will form a representation of the GP Eq. (2) only if the computational parameters are so chosen that we run the code in diffusion-like ordering:

$$\Delta t \sim \Delta x^2 \sim \varepsilon^2 \quad, \quad \text{and} \quad \Omega \to \varepsilon^2 \Omega \quad. \tag{20}$$

Under this ordering, the spinor time advancement yields:

$$\left| \phi(\mathbf{x}, t + \Delta t) \right\rangle = \left| \phi(\mathbf{x}, t) \right\rangle - i\varepsilon^2 \left[-\sigma_x \nabla^2 + \Omega \right] \left| \phi(\mathbf{x}, t) \right\rangle + O(\varepsilon^4) \tag{21}$$

To move to the GP Eq. (2), we take the zeroth moment of the spinor, defining

$$\psi(\mathbf{x}, t) = \begin{pmatrix} 1 & 1 \end{pmatrix} . \left| \phi(\mathbf{x}, t) \right\rangle = \gamma_{01}(\mathbf{x}, t) + \gamma_{10}(\mathbf{x}, t) \tag{22}$$

and defining

$$\Omega(\mathbf{x}, t) = V_{ext} + g \left| \psi(\mathbf{x}, t) \right|^2 \tag{23}$$

so that

$$i \frac{\partial \psi}{\partial t} = -\nabla^2 \psi + \left[V_{ext} + g|\psi|^2 \right] \psi + O(\varepsilon^2). \tag{24}$$

There are some important remarks that must be made about the QLG algorithm:

(a) QLG is a perturbative algorithm for non-linear problems,

(b) Since it is a lattice-based algorithm it will result in a finite difference representation of the GP Eq. (24) provided the parameters are so chosen to yield diffusion-like ordering,

(c) It might first be tempting to consider Trotter-like decompositions for higher order representations of the collision operator $\hat{C}_D$ - just as one is forced to do in Quantum Monte Carlo simulations of (equilibrium) Hubbard model problems. However this is totally counter productive for QLG. In QLG, all operator effects (from both streaming and further collision steps) are required to give higher order effects over the simple linear expansion for $\hat{C}_D$. These error terms are 2nd order, $O(\varepsilon^2)$ - exactly the error terms arises from the lattice discretization effects themselves.

(d) A consequence of this required ordering is that the GP order parameter $\psi(\mathbf{x}, t)$ must itself be small, with $\left| \psi(\mathbf{x}, t) \right| = O(\varepsilon)$.

(e) The GP Eq. (24) satisfies both conservation of particles and energy:

$$\int d^3x \left| \psi(\mathbf{x}, t) \right|^2 = N_0 = const. \quad ; \quad \int d^3x \left[\psi^* \left(-\nabla^2 + V_{ext} \right) \psi + \frac{1}{2} g|\psi|^4 \right] = E = const. \tag{25}$$

The computational QLG algorithm will indeed be satisfying the diffusion-like ordering in the Parameters if both N_0 and E are conserved during the run.

It is straightforward to extend the QLG to spinor BECs or coupled BEC systems: the collide-stream $\hat{C}_D, \hat{S}$ interleaved sequence yields a second order accurate lattice representation of the operator $i\partial/\partial t + \nabla^2$, while the potential term (in the collision operator) is an "inert" term giving the nonlinear couplings. Our original QLG algorithm split the nonlinear terms from the collision operator: in this algorithm, the collision operator was simply the unitary square-root-of-swap gate

$$\hat{C}_{swap} = \frac{1}{2}\begin{pmatrix} 1-i & 1+i \\ 1+i & 1-i \end{pmatrix} = \exp\left[i\frac{\pi}{4}\sigma_x(1-\sigma_x)\right] \text{ with } \hat{C}^2_{swap}\begin{pmatrix} \gamma_{01} \\ \gamma_{10} \end{pmatrix} = \begin{pmatrix} \gamma_{10} \\ \gamma_{01} \end{pmatrix}. \qquad (26)$$

What is interesting to note about this old algorithm is that $\hat{C}^4_{swap} = \hat{I}$, and the interleaving non-commutivity of $\hat{J}^2_{x0} = \hat{S}_{-\Delta x,0}\hat{C}_{swap}.\hat{S}_{+\Delta x,0}\hat{C}_{swap}.\hat{S}_{-\Delta x,0}\hat{C}_{swap}.\hat{S}_{+\Delta x,0}\hat{C}_{swap}$ is what keeps $\hat{J}^2_{x0} \neq \hat{I}$. It is thus somewhat reminiscent of the elements of a Lie algebra which lie infinitesimally close to the identity operator.

Benchmarking Against 1D Vector Soliton Collisions

We have performed some benchmarking runs against exactly soluble 1D vector soliton collisions. Consider a coupled set of 1D NLS equations

$$i\frac{\partial Q_1}{\partial t} = -\frac{\partial^2 Q_1}{\partial x^2} - 2\mu\left(|Q_1|^2 + B|Q_2|^2\right)Q_1, \qquad i\frac{\partial Q_2}{\partial t} = -\frac{\partial^2 Q_2}{\partial x^2} - 2\mu\left(|Q_2|^2 + B|Q_1|^2\right)Q_2 \qquad (27)$$

where Q_1, Q_2 are the electric field polairzations of a single mode propagating down an optical birefringent optical medium, with cross phase birefringence coefficient B that couples to the two polarizations. For these so-called Manikov solitons one can find some initial vector soliton amplitudes that will yield an inelastic collision: i.e., for a unique set of amplitudes the first post-collision amplitude for one of the solitons of Q_1 will be zero. However for nearly all other collisions there are always 2 solitons for each polarization (Figs 7 and 8).
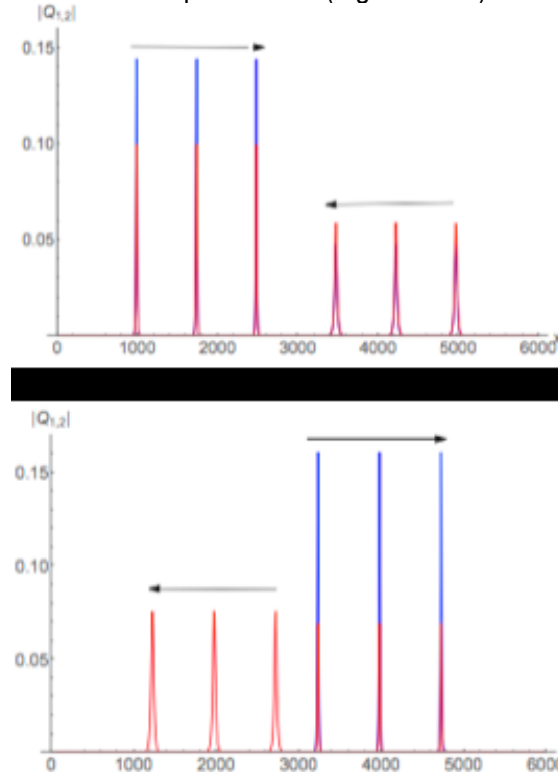

Fig. 7 The 1st vector soliton collision. Initially both polarizations have a 2-soliton state (Q_1 in blue, Q_2 in red) : one a left traveling soliton (at x = 1000) and the other a right traveling soliton (at x = 5000). The upper plot is the pre-collision solitons at 3 snapshots. The lower plot is the1st-post

collision soliton. Note that during this 1st post-collision state there is destruction of the left-traveling soliton for Q_1.

This is possible because the normalization constraint

$$\int dx \left| Q_i \right|^2 = \text{const.} = c_i \ , \ \ i = 1,2 \tag{28}$$

can still be satisfied by a 2-soliton for each polarization. This, of course, is not possible for a scalar vector soliton with its 1-soliton state and its non-zero normalization.

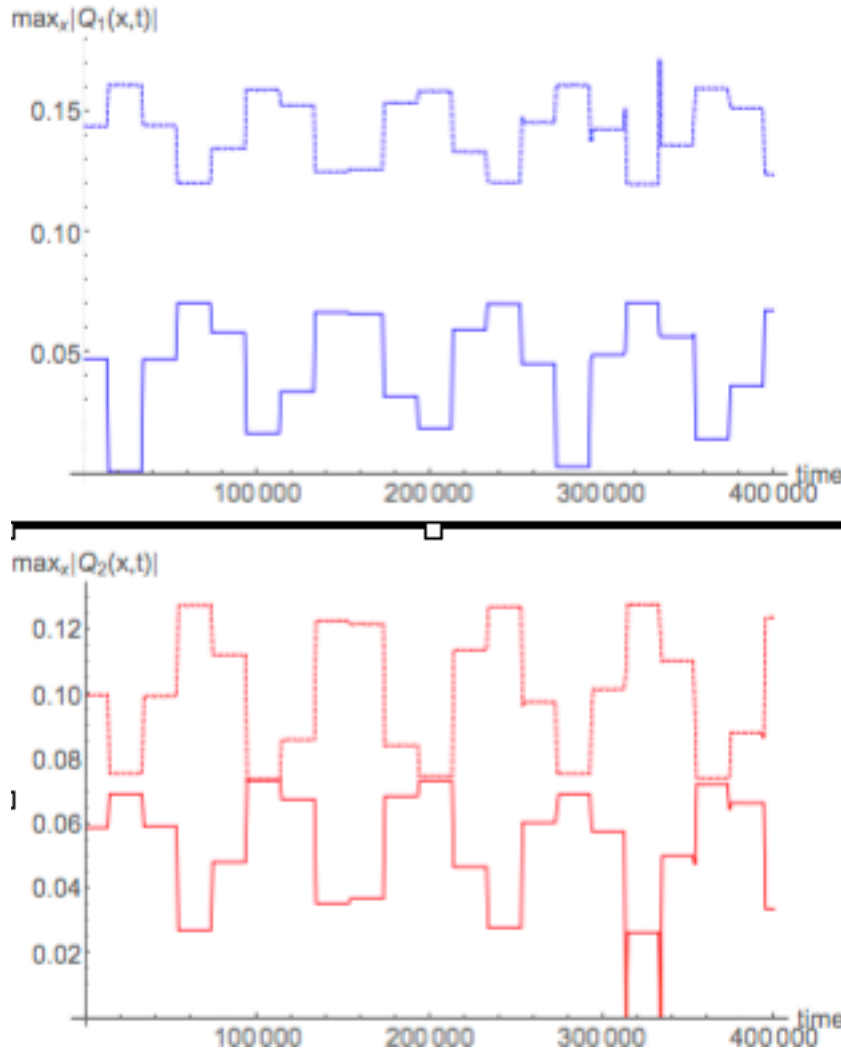In Fig. 8 we plot the maximum amplitudes of the 2-solitons for each of the polarizations for 21 collisions.

Fig. 8 The plot of the local maxima for the 2-solitons for each polarization (Q_1 in blue, Q_2 in red) in 21 collisions. Note that only for the 1st collision is the left-traveling soliton annihilated if the unique initial set of amplitudes appropriately selected.

Parallelization of QLG algorithms

The beauty of the QLG algorithm will not only run on a quantum computer when they become available because of its unitarity structure, but it is highly parallelizeable on classical supercomputers. We comment on both strong and weak scaling timings : in strong scaling one fixes the grid and increases the number of cores. For ideal parallelization, the wallclock time will decrease by a factor of two if the number of cores are doubled. In weak scaling, the amount of computation is kept fixed: the factor increase in the lattice grid is matched by the factor increase in the number of cores.

On the Oak Ridge National Laboratory CRAY XK7, TITAN , we ran up to 288,000 cores on grid. For strong scaling we find parallelization efficiency of an excellent 99.2%

Cores	Wallclock (s)	Ideal (s)	Speed-up [ideal]
150 000	974.13	974.13	1.00 [1.00]
240 000	613.45	608.83	1.59 [1.60]
288 000	511.24	507.36	1.91 [1.92]

Table 1 Strong scaling on TITAN, CRAY XK7 using 9600^3

Weak scaling is also excellent, as we scale from a 1600^3 grid with 4096 cores to 6400^3 grid with 262 144 cores.

Grid	Cores	Wallclock (s)	Ideal (s)
1600^3	4 096	332.33	332.33
3200^3	32 768	334.08	332.33
4800^3	110 592	332.85	332.33
6400^3	262 144	334.48	332.33

Table 2 Weak scaling on TITAN, CRAY XK7

The problem we encountered with our QLG algorithm on the CRAY XK7 is the low computational intensity of our code. Thus we could not use the GPUs efficiently on the CRAY XK7 – seeing saturation effects on thousands of CPU/GPU chips. Basically, as originally designed, the original GPU chips did not communicate with each other.

On the Argonne National Laboratory, we have been able to run at 1.17 Peta Flops using 2/3rds of the full IBM BG/Q , *MIRA*. Strong scaling to the full 786 432 cores is excellent, using 9600^3 core

#nodes	Ranks – Mode C32	Time (s)	Speed-up [ideal]
16 384	524 288	817.1	1.0 [1.0]
32 768	1 048 576	389.7	2.1 [2.0]
49 152	1 572 864	275.8	3.0 [3.0]

Table 3 Strong scaling on IBM BG/Q MIRA using 9600^3.

The weak scaling on *MIRA* is again excellent.

Grid	Nodes	Ranks – Mode C16	Time (s)
800^3	32	512	323.4
1600^3	256	4 096	323.4
3200^3	2 048	32 768	323.7
6400^3	16 384	262 144	326.5

Table 4 Weak scaling on the IBM BG/Q MIRA   using 1 MPI rank/core

Grid	Nodes	Ranks – Mode C16	Time (s)
800^3	32	2 048	203.7
1600^3	256	16 384	197.1
3200^3	2 048	131 072	197.8
6400^3	16 384	1 048 576	209.6

Table 5 Weak scaling on the IBM BG/Q MIRA   using 4 MPI rank/core

The strong scaling, with OpenMP timings on a 5120^3-grid on 32 (out of a maximum of 48) racks, yields a parallel efficiency 94.1% with a 1.17 Peta Flops:

	4 ranks	8 ranks	16 racks	32 racks
Wallclock (s)	406.11	203.62	106.58	53.94
Cores	65 536	131 072	262 144	524 288
Parallel Efficiency	100%	99.7%	95.3%	94.1%
L1 d-cache	88.64%	89.13%	89.11%	88.79%
DDR	2.59%	2.51%	2.56%	2.63%
GFlops/node	38.42	38.35	36.34	36.12
PFlops	0.156	0.311	0.595	1.174

Table 6   Strong scaling on the IBM BG/Q MIRA using OpenMP on 5120^3

Finally, we present scaling on ERDC's SGI ICE X *TOPAZ* that we achieved in our successful competition to be given CAP-2 allocation.

Cores	Wallclock	Speed-up	Ideal
13 824	3515.90	1.00	1.00
27 000	1792.63	1.96	1.95
36 000	1343.39	2.62	2.60
52 920	917.18	3.83	3.83
74 088	655.49	5.36	5.36

Table 7   Strong scaling on SGI ICE X TOPAZ (ERDC) on grid 4200^3.

Similarly, for weak scaling we find excellent scaling.

Grid	Cores	Wallclock (s)	Ideal (s)
600^3	216	648.08	648.08
1200^3	1 728	647.48	648.08
1800^3	5 832	646.38	648.08
2400^3	13 824	647.27	648.08
3600^3	46 656	654.31	648.08
4200^3	74 088	655.49	648.08

Table 8 Weak scaling on the SGI ICE X TOPAZ (ERDC)

QLG for SPINOR BECs

If a spin-2 ^{87}Rb BEC is trapped in a magnetic well, the spin degrees of freedom are frozen along the magnetic field and the T = 0 mean field theory of this BEC is given by the scalar GP Eq. (24). However, if the spin-2 BEC is trapped in an optical well then the spin degrees of freedom require a spinor-GP mean field theory representation. For spin-2 this results in 5 coupled GP Eqs., with the spinor wave function $\Psi = \begin{pmatrix} \psi_{-2} & \psi_{-1} & \psi_0 & \psi_1 & \psi_2 \end{pmatrix}^T$. The Hamiltonian is now given by

$$H = \int d^3x \left[\sum_{m=-2}^{2} \psi_m^* \left(-\nabla^2 + V_{ext} \right) \psi_m + \frac{1}{2}c_0 n^2 + \frac{1}{2}c_1 |\mathbf{F}|^2 + \frac{1}{2}c_2 |A|^2 \right] \tag{29}$$

where the mean density

$$n(\mathbf{x},t) = \sum_{m=-2}^{2} |\psi_m(\mathbf{x},t)|^2 , \tag{30}$$

the spin vector density

$$\mathbf{F}(\mathbf{x},t) = \sum_{m,n=-2}^{2} \psi_m^*(\mathbf{x},t) \mathbf{f}_{m,n} \psi_n(\mathbf{x},t) \tag{31}$$

and $\mathbf{f}_{m,n}$ are the components of the 5x5 spin-2 matrices, with $\mathbf{f}_{m,n} = \left(f_{m,n}^x , f_{m,n}^y , f_{m,n}^z \right)$, and $A(\mathbf{x},t)$ is the singlet-pair amplitude

$$A(\mathbf{x},t) = \sum_{m=-2}^{2} (-1)^m \psi_m(\mathbf{x},t) \psi_{-m}(\mathbf{x},t) \tag{32}$$

When there is a phase transition from normal to BEC there is a change in symmetry properties under parameter variations.   It was finally understood that the spinor wave function Ψ is the order parameter for the system. Let *G* be the group which leaves the energy functional *H*, Eq. (29), invariant and *H* the invariant subgroup that leaves the wave function Ψ. The factor group *G/H* is the order parameter manifold with topologically invariant defects ("quantum vortices").

The physics of quasi Nambu-Goldstone modes [Uchino et. a. 2010] is of major importance in determining the low energy behavior of various systems with spontaneous symmetry breaking. This occurs in nearly all branches of physics, particularly with phase transitions. The signature – i.e., the so-called "charge" – of the topological defect/quantum vortex is defined by how the order parameter changes in a closed path around the defect. This will dictate how various equivalence classes of vortices will interact and reconnect. For a scalar BEC, the order parameter manifold is just the unitary group U(1), the circle group consisting of all complex numbers with absolute value 1 under multiplication. The topologival invariants are the additive group of integers – an Abelian group. The quantum vortices are singular vortices with zero density at their cores: $. \rho = |\psi|^2 = 0$, and the circulation about the cores are quantized.

However for BEC in an optical lattice, with the order parameter being the spinor wave function much more complex topological defects occur – in particular coreless vortices (skyrmions), vortices with rational superfluid circulation quantization (reminiscent of the fractional quantum Hall effect), and even unquantized circulation.

In particular we have followed the evolution of 2 interlaced skyrmions in an external potential. Here we will be dealing with non-singular coreless vortices with 2 coupled GP equations for the order parameter wave function $\Psi = \begin{pmatrix} \psi_+ & \psi_- \end{pmatrix}^T$: the ψ_+ - core (where its density is zero) is a vortex ring and is shown in green, while the ψ_- - core involves a standard line core region which then folds out into a torus (shown in orange). We report on the simulation of 3 interlaced skrymions, Fig. 10. In Fig. 9 we show the order parameter manifold for 2 such skrymions
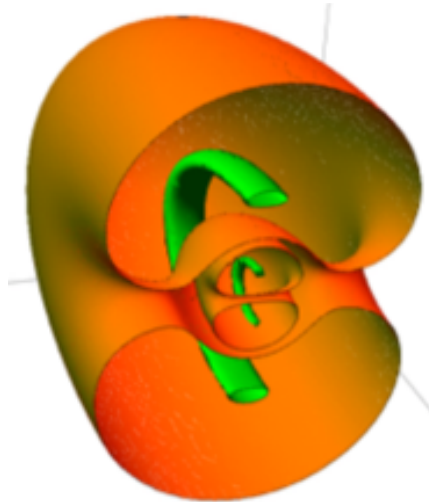
Fig. 9 The order parameter manifold for the two interlaced skrymions, with the component ψ_+ in green and ψ_- in orange.

In Fig. 10, we notice that the time evolution of the ψ_+-core component expands from a vortex ring into a capula with the absorption of the inner structures.

Fig. 10 The time evolution of 3 interlaced skyrmions cores. ψ_+ (green)-component core is initially a vortex ring which then evolves into a single coupla. The ψ_- (orange)-component core consists of a linear line core which folds onto itself toroidally. As time evolves the inner skyrmions are absorbed into a final single skyrmion.
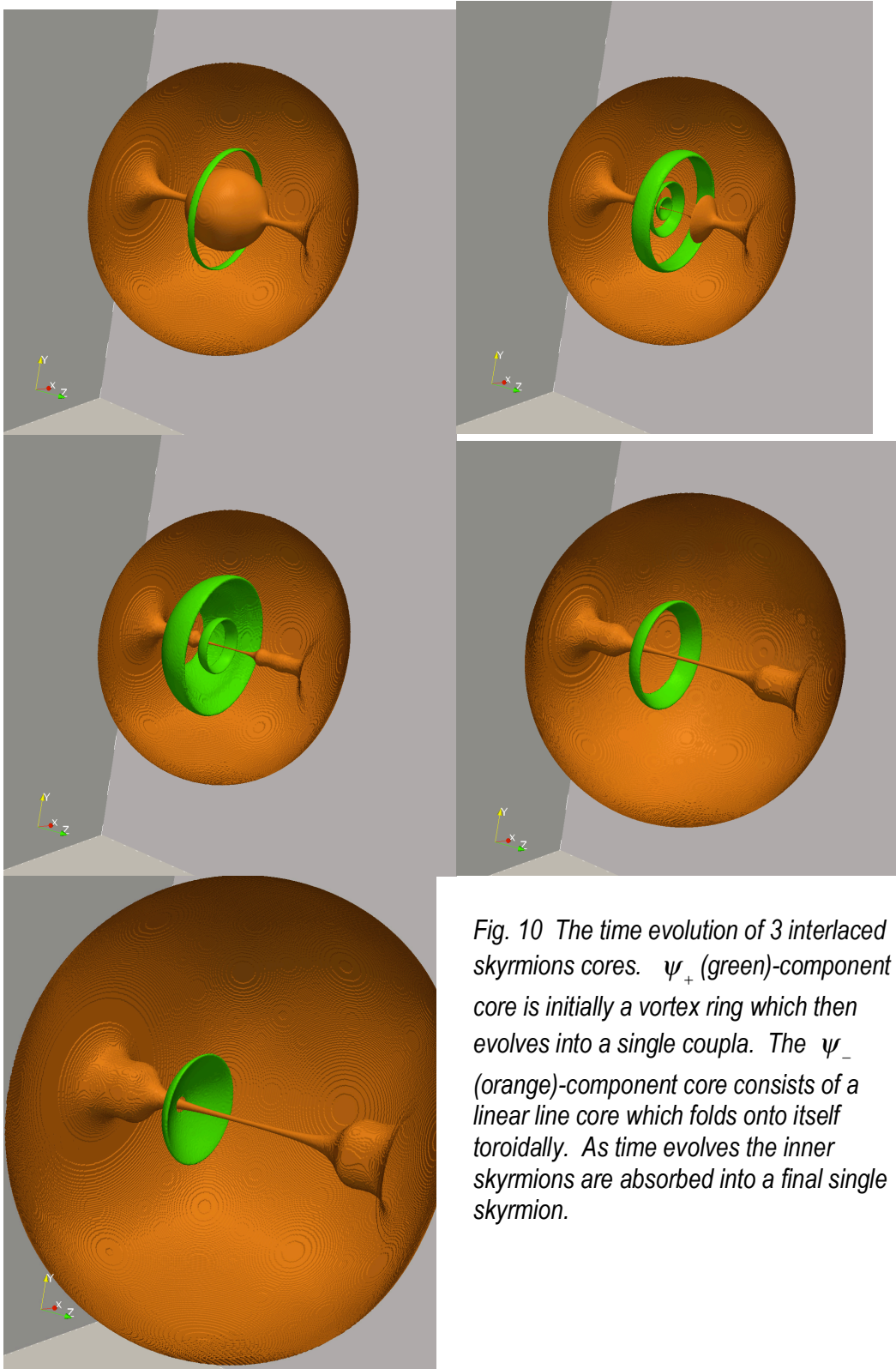
The spectra for these components are shown in Fig. 11

(a) spectra for vortex rings,   (b) spectra for linear core with its toroidal envelope
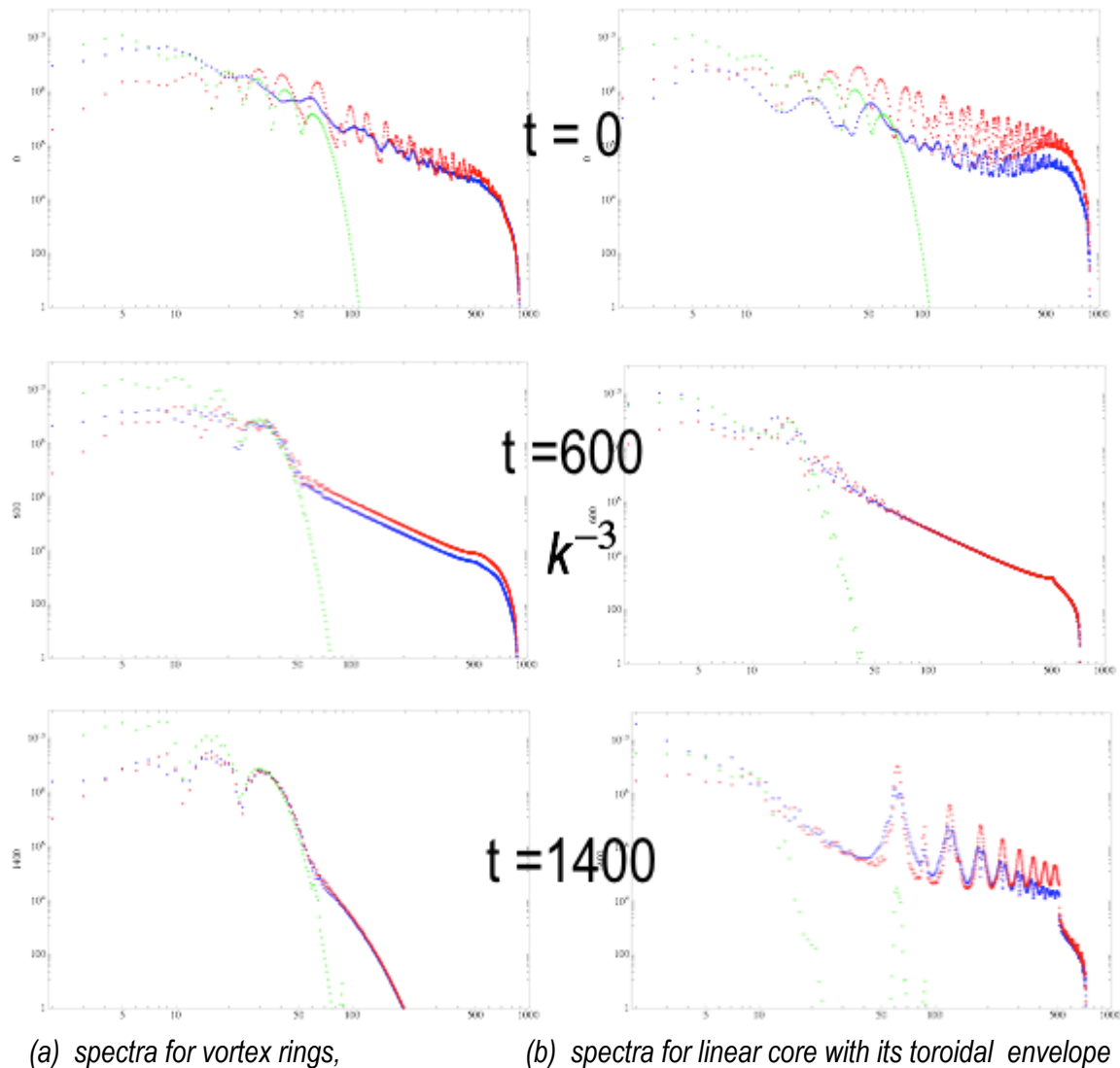
Fig. 11 the change in the spectrum for (a) vortex ring component and (b) linear vortex core with its
toroidal closure. The blue curves are the kinetic energy spectra, while the red curves are the
quantum energy spectrum.

• Spin-1 BEC VORTEX RECONNECTIONS

We have just started looking into vortex reconnections in spinor BECs. First, we consider spin-1 BEC. The Hamiltonian for the spin-1 BEC is basically that of Eq. (29) , except there is no singlet-pair interaction (i.e., $c_2=0$) and the summation over m now runs from m = -1 to + 1.

First consider the case where there is no spin-spin interaction, so that we only have the standard weak Boson-Boson coupling interactions :

$$c_1 = 0$$

Consider 4 mutually orthogonal vortices for m = -1 , 0, and +1. We find that if there are no spin-spin interactions among the *m – components* there are no vortex-vortex reconnecetions: in each m-component the line vortices remain constant (but with a slight expansion since these linear line vortices are not steady state solutions of the coupled spinor GP equations), Fig. 12
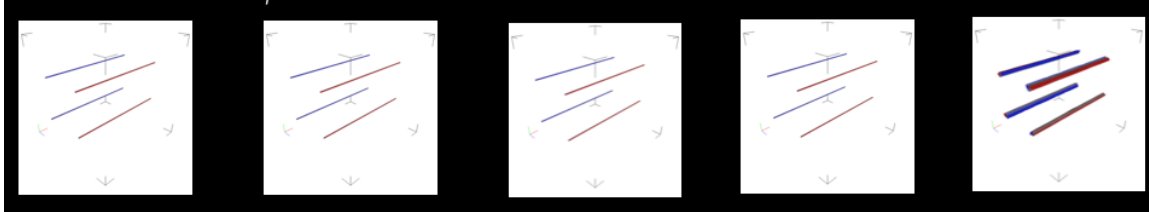
Fig. 12   The evolution of 4 parallel vortices in the y-direction for the m=0 spinor component. (The m = 1 spinor component has similar evolution for its 4 parallel vortices in the x – direction. Similarly for the m = -1 spinor component.)
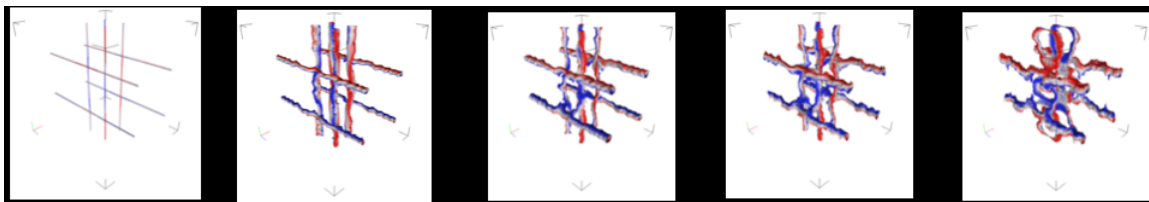
Now suppose for the initial conditions we permit only for the m = -1 spinor component to have within it orthogonal vortices. As expected one now finds vortex-vortex reconnection, but only within this spinor component, Fig. 13. This is exactly what one finds for scalar BEC vortex-vortex reconnection. These vortices are Abelian.

Fig. 13 The evolution of the m = - 1 spinor component with orthogonal vortices. One now finds vortex-vortex reconnection.   There is no reconnection in the m = 0 and m = +1 spinor components which just consist of 4 parallel vortices , orthogonal for each component.

We now include the effect of the spin-spin interaction term, $c_1 \neq 0$, in the Hamiltonian Eq. (29) on the vortex-vortex reconnection for the Abeiian spin-1 BEC. Consider purely orthogonal 4-vortices in each of the three component, as in Fig. 12 [in Fig. 12 there was no spin-spin interaction term and no vortex-vortex interaction]. Initially the m = -1 four line vortices are parallel to the x-axis while the m = 0 four line vortices are parallel to the y-axis and similarly the m = +1 four line vortices along the z-axis. We see rung vortices form in the reconnection in each component.

m = -1   m = 0   m = +1
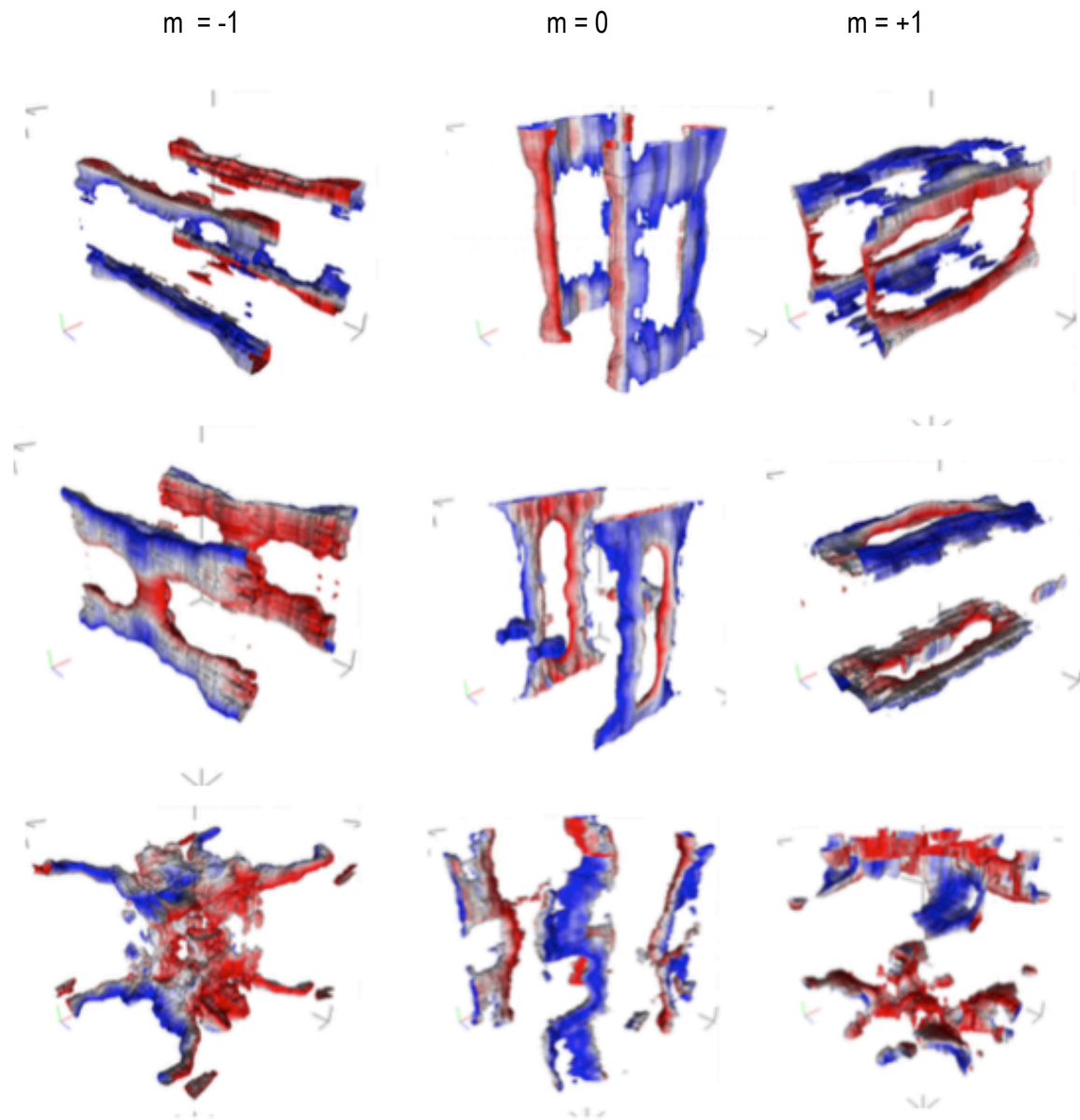
Fig. 14 The effect of the spin-spn interaction for the spin-1 BEC with initially orthogonal line vortices – this is the counterpart to Fig. 12 in which there was no spin-spin interaction in the Hamiltonian and no vortex-vortex reconnection. In the left column we have the time evolution of the reconnection (time increasing in the downward vertically direction). There is phase information on the vortex lines : blue: zero phase, red: phase 2*pi.

References

[1] "Quantum Lattice Gas Representation of Some Classical Solitons"
      G. Vahala, J. Yepez and L. Vahala
      Phys. Lett. A310, 187-196 (2003)

[2] "Lattice Boltzmann and Quantum Lattice Gas Representation of One-Dimensional
      Magnetohydrodynamic Turbulence
      L. Vahala, G. Vahala and J. Yepez

[3] "Quantum lattice gas representation for vector solitons"
      G. Vahala, L. Vahala, and J. Yepez
      SPIE Conf. Proc. 5105, 273-281 (2003)

[4] "Inelastic Vector Soliton Collisions: A Quantum Lattice Gas Representation"
      G. Vahala, L. Vahala and J. Yepez
      Phi. Trans. Roy. Soc. London 362, 1677-1690 (2004)

[5] "Quantum lattice gas representation of dark solitons"
      G. Vahala, L. Vahala and J Yepez
      SPIE Conf. Proc. 5436, 376-385 (2004)

[6] "Quantum Lattice Representation of 1D MHD turbulence with arbitrary Transport Coefficients"
      J. Yepez, G. Vahala and L. Vahala
      SPIE Conf. Proc. 5815, 227-235 (2005)

[7] "Scientific Visualization as Part of the Computational Model Development Process"
      S. Ziegeler, G. Vahala, L. Vahala, and J. Yepez
      NAVO Navigator, p. 19-23, (2005)

[8] "Non-local Closure and Parallel Performance of Lattice Boltzmann Models for Some Plasma
      Physics Problems"
      A.I.D. Macnab, G. Vahala, L. Vahala, J. Carter, M. Soe and W. Doland
      Physica A362, 48-56 (2006)

[9] "Quantum Lattice Representations for Vector Solitons in External Potentials"
      G. Vahala, L. Vahala an J. Yepez
      Physcia A362, 215-221 (2006)

[10] "Lattice Quantum Algorithm for the Schrodinger Wave Equation in 2+1 Dimensions with a
Demonstration by Modeling Soliton Instabilities"
      J. Yepez, G. Vahala and L. Vahala
      Quantum Info. Process. 4, 457-469 (Dec 2005)

[11] "Quantum Lattice Gas Algorithm for Quantum Turbulence and Vortex Reconnection in the Gross- Pitaevskii Equation"
  G. Vahala, J. Yepez and L. Vahala, , Proc. SPIE, 6976, 69760U1-10 (2008)

[12] "Vortex-antivortex pair in a Bose-Einstein condensate, J. Yepez, G. Vahala and L. Vahala, Eur. Phys. J. Special Topics 171, 9-14 (2009)

[13] "Superfluid Turbulence from Quantum Kelvin Wave to Classical Kolmogorov Cascades",
  J. Yepez, G. Vahala, L. Vahala and M. Soe,
  Phys. Rev. Lett. 103, 084501 (2009)

[14] "Unitary quantum lattice gas representation for 2D quantum turbulence",
  B. Zhang, G. Vahala, L. Vahala, M. Soe,
  Proc. SPIE 8057, 80570E1-12 (2011)

[15] "Unitary quantum lattice algorithm for two-dimensional quantum turbulence",
  B. Zhang, G. Vahala, L. Vahala, M. Soe,
  Phys. Rev. E84, 046701 (2011)

[16] "Poincare recurrence and spectral cascades in three-dimensional quantum turbulence",
  G. Vahala, J. Yepez, L. Vahala, M. Soe, B. Zhang and S. Ziegeler
  Phys. Rev. E84, 046713 (2011)

[17] "Unitary qubit lattice simulations of multiscale phenomena in quantum turbulence",
  M. Soe, G. Vahala, L. Vahala and J. Yepez.
  Supercomputing 2011, paper TCC304, Nov. 2011 (Seattle)

[18] "Qubit lattice (QLG) simulations for a T > 0 superfluid",
  G. Vahala, B. Zhang, L. Vahala, M. Soe and S. Ziegeler
  DoD High Performance Computing, User Group Conference, 2011

[19] "Unitary Qubit Lattice Gas Representation of 2D and 3D Quantum Turbulence",
  G. Vahala, B. Zhang, J. Yepez, L. Vahala and M. Soe,
  Chpt. 11 (pp. 239 - 272), in *Advanced Fluid Dynamics,* ed. H. W. Oh, (InTech Publishers, Croatia, 2012)

[20] "Unitary qubit lattice simulations of complex vortex structures",
  G.Vahala, J. Yepez, L. Vahala and M. Soe,
  Computat. Sci & Discovery, 5, 014013 (2012)

[21] Y. Kawaguchi and M. Ueda, *Spinor Bose-Einstein condensates* , Physics Reports 520, 253-381 (Nov. 2012); M. Ueda, *Fundamentals and New Frontiers of Bose-Einstein Condesnation* (World Sci.Publ., Singapore 2010)

[22] J. R. Abo-Shaeer, C. Raman, J. M. Vogels and W. Ketterle, Science 292, 476 (2001)

[23] C. F. Barenghi, Physica D 237, 2195 (2008); A. W. Baggaley and C. F. Barenghi, Phys. Rev. B83, 134509 (2011); A. W. Baggaley. C. F. Barenghi, A. Shukurov and Y. A. Sergeev, Europhys. Lett. 98, 26002 (2012); E. Kozik and B. Svistunov, Phys. Rev. Lett. 92, 035301 (2004); G. Boffetta, A. Celani, D. Dezzani, J. Laurie and S. Nazarenko, J. Low Temp. Phys. 156, 193 (2009); V. S. L'vov and S. V. Nazarenko, arXiv:1208.4593 (2012); E. B. Sonin, Phys. Rev. B85, 104516 (2012); L. Laurie, V. S. L'vov, S. Nazarenko and O. Rudenko, Phys. Rev. B81, 104526 (2010); V. S. L'vov and S. Nazarenko, JETP Lett. 91, 428 (2010); E. Kozik and B. V. Svistunov, Phys. Rev. B82, 140510 (2010); A.W. Baggaley and C. F. Barenghi, Phys. Rev. B83, 134509 (2011); V. V. Lebedev, V. S. L'vov and S. V. Nazarenko, J. Low Temp. Phys. 161, 606 (2010); V. S. L'vov, S. V. Nazarenko and O. Rudenko, Phys. Rev. B76, 024520 (2007); G. Krstulovic and M. Brachet, Phys. Rev. Lett. 106, 115303 (2011); V. S. L'vov, S. V. Nazarenko and O. Rudenko, Phys. Rev. B76, 024520 (2007); E, V, Kozik and B. V. Svistunov, J. Low Temp. Phys. 161, 603 (2010); N. Sasa, T. Kano, M. Machida, V. S. L'vov, O. Rudenko and M. Tsubota, Phys. Rev. B84, 54525 (2011); M. Kobayashi and M. Tsubota, Phys. Rev. Lett. 94, 065302 (2005); M. Tsubota, J. Low Temp. Phys. (to appear 2012); arXiv:1207.3589v1; N. Sasa, T. Kano, M. Machida, V. S. L'vov, O. Rudenko and M. Tsubota, Phys. Rev. B84, 54525 (2011); G. P. Bewley, D. P. Lathrop and K. r. Sreenivasan, Nature 441, 588 (2006); M. S. Paoletti, R. B. Fiorito, K. R. Sreenivasan and D. P. Lathrop, J. Phys. Soc. Japan 77, 111007 (2008); M S. Paoletti, M. E. Fisher and D. P. Lathrop, Physica D239, 1367 (2010); M. Kobayashi and M. Tsubota, Phys. Rev. A76, 045603 (2007); E. A. L. Henn, J. A. Seman, G. Roati, K. M. F. Magalhaes and V. S. Bagnato, Phys. Rev. Lett. 103, 045301 (2009); H. Taakeuchi, S. Ishino and M. Tsubota, Phys. Rev. Lett. 105, 205301 (2010); S. Ishino, M. Tsubota and H. Takeuchi, Phys. Rev. A83, 063602 (2011)

[24] S. Uchino, M. Kobayashi, M. Nitta and M. Ueda, Phys. Rev. Lett. 105 , 230406 (2010)

[25] A. Oganesov, G. Vahala, L. Vahala, J. Yepez, M. Soe & B. Zhang, "Unitary quantum lattice gas algorithm generated from the Dirac collision operator for 1D soliton-soliton collisions, REDS Plasma Science & Plasma Tech 170, 55-64 (2015)

[26] A. Oganesov, G. Vahala, L. Vahala, J. Yepez, & M. Soe, "Benchmarking the Dirac-Generated unitary lattice qubit collision-stream algorithm for 1D vector Manakov soliton collisions", Computers & Math. With Applications (on-line, June 2015)

1.

1. Report Type

Final Report

Primary Contact E-mail
Contact email if there is a problem with the report.

gvahala@gmail.com

Primary Contact Phone Number
Contact phone number if there is a problem with the report

757-495-1158

Organization / Institution name

William & Mary

Grant/Contract Title
The full title of the funded effort.

Unitary Quantum Lattice Algorithms for Turbulence

Grant/Contract Number
AFOSR assigned control number. It must begin with "FA9550" or "F49620" or "FA2386".

FA9550-13-1-0038

Principal Investigator Name
The full name of the principal investigator on the grant or contract.

©eorge Vahala

Program Manager
The AFOSR Program Manager currently assigned to the award

Fariba Fahroo

Reporting Period Start Date

02/15/2013

Reporting Period End Date

02/14/2016

Abstract

A qubit unitary lattice algorithm is developed for the mean field evolution of the ground state of a Bose-Einstein condensate – whether in a magnetic or optical trap. The algorithm consists of interleaved collide-stream operators which in diffusion ordering recovers the spinor Gross Pitaevskii equations and is ideally parallelized. The algorithm is benchmarked against exact one dimensional vector inelastic soliton collision solutions. Only for a unique set of initial amplitudes is there inelastic collision of these vector solitons. Our algorithm was then followed for over 21 soliton collisions without loss in accuracy. Three dimensional quantum turbulence was examined for scalar Bose Einstein condensates and the compressible kinetic energy spectrum was shown to exhibit three different cascades – indicative of three different length scales. We identified these as the classical regime (where the spectrum exhibited the Kolmogorov -5/3 spectrum of classical incompressible turbulence), a semiclassical regime and a quantum regime with a strong -3 spectral exponent). The incompressible kinetic energy exhibits basically only a -3 spectrum throughout the whole wave number range, indicative of the fact that the singular vortex core exhibit zero density at the core. Spinor BEC vortex-vortex collisions are then examined for spin-1 systems and it is shown that the spin-spin interaction term in the Hamiltonian is critical for reconnection: without the spin-spin interaction term the vortices are oblivious to each other. The evolution of nested skyrmions, with coreless vortices consisting of a vortex ring and a straight line vortex that closes on itself on a toridal manifold. Under period

boundary conditions one finds a lattice of mini-skyrmions perculating the field.

Distribution Statement

This is block 12 on the SF298 form.

Distribution A - Approved for Public Release

Explanation for Distribution Statement

If this is not approved for public release, please provide a short explanation. E.g., contains proprietary information.

SF298 Form

Please attach your SF298 form. A blank SF298 can be found here. Please do not password protect or secure the PDF The maximum file size for an SF298 is 50MB.

SF298.pdf

Upload the Report Document. File must be a PDF. Please do not password protect or secure the PDF . The maximum file size for the Report Document is 50MB.

AFOSR_Final_Report.pdf

Upload a Report Document, if any. The maximum file size for the Report Document is 50MB.

Archival Publications (published) during reporting period:

Changes in research objectives (if any):

Change in AFOSR Program Manager, if any:

Extensions granted or milestones slipped, if any:

AFOSR LRIR Number

LRIR Title

Reporting Period

Laboratory Task Manager

Program Officer

Research Objectives

Technical Summary

Funding Summary by Cost Category (by FY, $K)

	Starting FY	FY+1	FY+2
Salary			
Equipment/Facilities			
Supplies			
Total			

Report Document

Report Document - Text Analysis

Report Document - Text Analysis

Appendix Documents

2. Thank You

E-mail user

May 11, 2016 17:11:11 Success: Email Sent to: gvahala@gmail.com